An EMG-Driven Weight Support System With Pneumatic Artificial Muscles

Jun-ichiro Furukawa, Tomoyuki Noda, Tatsuya Teramae, and Jun Morimoto

***Abstract*—In this paper, we introduce our newly developed biosignal-based vertical weight support system that is composed of pneumatic artificial muscles (PAMs) and an electromyography (EMG) measurement device. By using our developed weight support system, assist force can be varied based on measured muscle activities; most existing systems can only generate constant assist forces. In this paper, we estimated knee and ankle joint torques from measured EMGs using floating base inverse dynamics. Knee and ankle joint estimated torques are converted to vertical forces by the kinematic model of a subject. The converted vertical forces are used as force inputs for the PAM actuator system. To validate our system's control performance, four healthy subjects performed a one-leg squat with his left leg while his right leg was assisted by our proposed system. We used the vertical force estimated from the measured EMG signals as a control input to the weight support system. We compared EMG magnitudes with four different experimental conditions: 1) normal two-leg squat; 2) one-leg squat without the assist system; 3) one-leg squat with EMG-based weight support; and 4) one-leg squat with constant force support. The EMG magnitude with the proposed weight support system was much closer to that with normal two-leg squat than that with one-leg squat without the assist system and than that with one-leg squat with constant force support.**

***Index Terms*—Electromyography (EMG), force control, pneumatic actuators, rehabilitaion robotics, weight support system.**

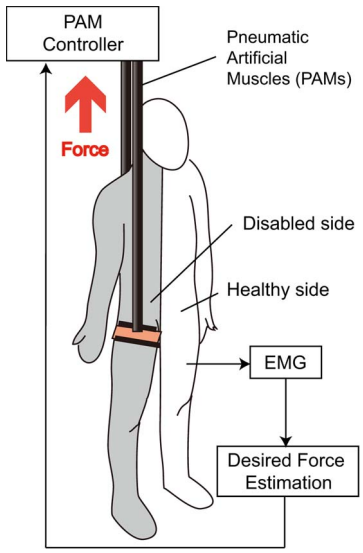

Fig. 1. Schematic of our proposed weight support system. Upward and downward movements are assisted with the force estimated from measured electromyography (EMG).

I. Introduction

WEIGHT support is essential in rehabilitation for lower limbs, where standing up, stepping, walking, or balancing movements can be involved. In conventional weight support systems, assist force is typically constant, and operational height ranges are limited. Therefore, weight support devices have only been used for safety or fault tolerance instead of actively changing amount of weight support. On the other hand, for active weight and movement support, research attention on the development of an exoskeleton robot is increasing [1]–[6]. However, it remains difficult for therapists to work with such systems since exoskeleton robots generally require complicated setups. In this paper, we propose a weight support system that has a wider operational range and can adaptively change the amount of support rather than simply generating constant force. To satisfy the aforementioned specifications, we used pneumatic artificial muscles (PAMs) with force sensors and a device to measure the PAM length. PAMs are used for robotics applications [6]–[10]. Fig. 1 shows a schematic of our proposed weight support system.

To adaptively change the weight support force based on the subject's status, a user's movement intention must be estimated. For predicting user movements to control assistive devices, EMGs are commonly used [1], [4], [11]–[18]. In this paper, we estimate knee and ankle joint torque from measured EMGs. We first simultaneously measure the joint angle trajectories and the EMG profiles of a subject. Then, the torque sequence that corresponds to the measured joint angle trajectories is derived using inverse dynamics. Although previous studies also used inverse dynamics to estimate knee-joint torque from EMG signals, the knee movements were generated when a subject was sitting [19], [20]. To deal with such daily life related behaviors as squat movements, we must explicitly consider the

Manuscript received October 11, 2013; revised March 13, 2014 and April 24, 2014; accepted June 7, 2014. Date of publication July 8, 2014; date of current version August 23, 2016. This research reflects the results of the "Development of BMI Technologies for Clinical Application" and "Brain Machine Interface Development" carried out under the Strategic Research Program for Brain Sciences by the Ministry of Education, Culture, Sports, Science and Technology of Japan. Part of this research was supported by MIC SCOPE and a contract with the Ministry of Internal Affairs and Communications entitled "Novel and innovative R&D making use of brain structures." This research was also partially supported by MEXT KAKENHI Grant Number 23120004, JSPS KAKENHI Grant Number 24700203 and Strategic International Cooperative Program, Japan Science and Technology Agency (JST) and by JSPA and MIZS: Japan Slovenia research Cooperative Program.

J. Furukawa is with the Graduate School of Frontier Biosciences, Osaka University, Osaka 565-0871, Japan and with the Department of Brain Robot Interface, ATR Computational Neuroscience Laboratories, Kyoto 619-0288, Japan (e-mail: furukawa@atr.jp).

T. Noda, T. Teramae, and J. Morimoto are with the Department of Brain Robot Interface, ATR Computational Neuroscience Laboratories, Kyoto 619-0288, Japan (e-mail: t_noda@atr.jp; t-teramae@atr.jp; xmorimo@atr.jp).

Digital Object Identifier 10.1109/JSYST.2014.2330376

ground reaction force in inverse dynamics. Therefore, we use floating base inverse dynamics [21].

To find the relationship between the target torque and the measured EMG signals, we built a real-time torque estimation model, which is composed of the Hill–Stroeve model [22], [23], to derive the muscle force from the measured EMGs and a pulley-tendon model to convert the muscle force to joint torque. The estimated torques of the knee and ankle joints are used to derive vertical forces using the subject's kinematic model. Finally, we used the derived vertical forces as force inputs for our PAM actuator system. To validate its control performance, a subject performed one-leg squats by his left leg while his right leg was assisted by our proposed system. We used the vertical force estimated from the knee and ankle movement related EMG signals measured by seven sensor channels as control input for the weight support system. We compared EMG magnitudes with four different experimental conditions: 1) normal two-leg squat; 2) one-leg squat without the assist system; 3) one-leg squat with EMG-based weight support; and 4) one-leg squat with constant force support. The EMG magnitude with our proposed weight support system was much closer to that with a normal two-leg squat than that with a one-leg squat without using the assist system.

The rest of this paper is organized as follows. In Section II, we introduce our newly developed weight support system that is composed of PAMs and an EMG measurement device. In Section III, we explain how we derive the assist force from the measured EMG signals. In Section IV, we introduce a calibration strategy for our weight support system and its experimental setups. In Section V, we show the results of squat experiments with four different conditions. We finally conclude in Section VI.

II. Weight Support System

A. PAM Actuators

To assist motions by estimated torques of the knee and ankle joints, we develop a weight support system (see Fig. 2), where the actuator is a paired PAMs.

We use 1.4-m-long PAM (FESTO Inc.), which has a diameter of 10 mm and 25% contraction rate from natural length. According to the specification provided by FESTO Inc., the PAM can generate 630-N maximum force. The system is about 0.8 kg without including air compressor and valve. In addition, the system can operate up to 0.5 Hz with the amplitude of 0.35 m. These specifications were experimentally validated as described in Section IV-A.

While PAM is lightweight, it can produce large force, converting pressured gas energy into contraction force through its rubber tubes. The force is generated by the path contraction of the spiral fiber expansion embedded by the pneumatic bladder. With proportional pressure valves, PAM pressure p can be controlled. The force generated by PAM depends on the pressure p and the contraction rate; the PAM force model [24], [25] is given by

$$f_{\text{pam}} = \frac{\pi D_0^2 p}{4}\left(\frac{3}{\tan^2\psi_0}(1-\varepsilon)^2 - \text{bias}\right) \tag{1}$$

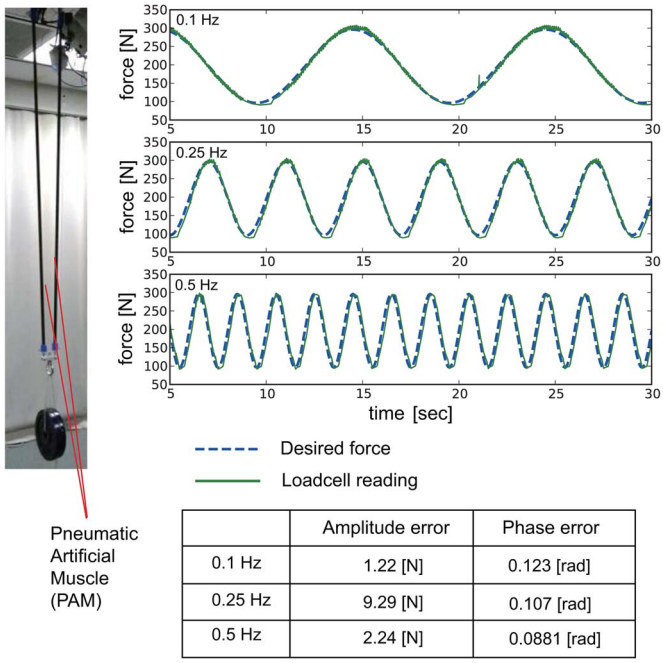

	Amplitude error	Phase error
0.1 Hz	1.22 [N]	0.123 [rad]
0.25 Hz	9.29 [N]	0.107 [rad]
0.5 Hz	2.24 [N]	0.0881 [rad]

Fig. 2. Torque tracking performance of PAM-based weight support system with frequencies of 0.1, 0.25, and 0.5 Hz. A thirty-kilogram weight was attached to the bottom of the support system.

where ε is the contraction rate of PAM, and D_0 and ψ_0 are the PAM diameter and the angle of the embedded spiral wire at the atmosphere pressure, respectively. This can be represented as a quadratic function multiplied with the current PAM pressure p, i.e.,

$$f_{\text{pam}} = g(\varepsilon, p) = p(a\varepsilon^2 + b\varepsilon + c) \tag{2}$$

where

$$a = \frac{3\pi D_0^2}{4\tan^2\psi_0}, \quad b = -\frac{3\pi D_0^2}{2\tan^2\psi_0}$$
$$c = \frac{\pi D_0^2}{4}\left(\frac{3}{\tan^2\psi_0} - \frac{1}{\sin^2\psi_0}\right). \tag{3}$$

If desired force f_{pam} needs to be generated at contraction rate ε, desired valve pressure p^* can be derived from the inverse model $p^* = g^{-1}(f_{\text{pam}}; \varepsilon)$.

B. EMG Measurement

We estimate the muscle force from ten sample histories of EMG signals, where the sampling period is $\Delta t = 4$ ms. In other words, we use a 40-ms sample history to estimate muscle force. Then, for the muscle force estimation, we consider an input variable

$$q_t^i = \frac{u_t^i}{u_{\max}^i} \tag{4}$$

where

$$u_t^i = \sum_{k=t-9}^{t} e_k^i \Delta t \tag{5}$$

where e_k^i represents low-pass filtered and full-wave rectified muscle activity measured by the ith EMG sensor channel at

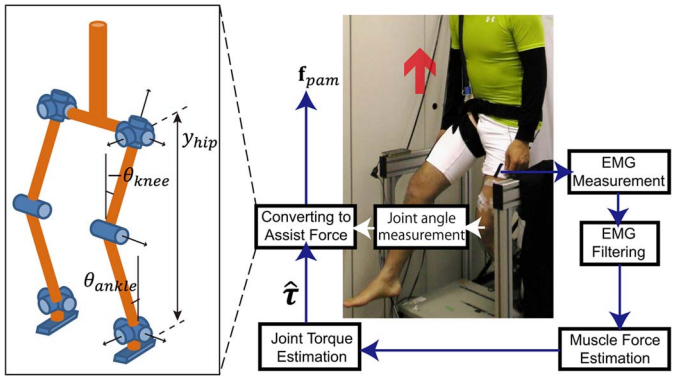

Fig. 3. Control strategy of the weight support system. Muscle forces are estimated from full-wave rectified and bandpass-filtered EMG signals. Joint torque $\hat{\boldsymbol{\tau}}$ is derived from the estimated muscle force by using the tendon-pulley model. Then, the derived torque is converted to desired assist force $f_{\rm pam}$ for PAM by taking measured joint angles into account.

time k with the cutoff frequency of 2 Hz. $u^i_{\max}$ is the measured maximum muscle activity to normalize an impedance change of an EMG electrode.

III. Method

Fig. 3 shows our control strategy of the proposed weight support system. First, we measure the EMG signals and the joint angles simultaneously from the left leg during the normal squat motion, and the parameters of the tendon-pulley model in (7) are estimated from the acquired EMG and joint angle data. Then, the online operation of the weight support system is as follows.

1) Online EMG and joint angle measurements during the motion.
2) Derive the muscle force from the Hill–Stroeve model.
3) Estimation of the knee and ankle joint torques by using the tendon-pulley model with the identified parameters.
4) Calculate the vertical assist force from the estimated knee and ankle joint torques by using the Jacobian matrix, which represents the relationship between the joint movements and a hip position movement.

A. Estimating Muscle Force

The muscle force is derived by using the Hill–Stroeve model [22], [23] from EMG signals. The model takes the nonlinearities of the muscle length–tension relationship and force–velocity relationship, i.e.,

$$f^i_t = k\left(\xi^i_t\right) h\left(\eta^i_t, \xi^i_t\right) \overline{f^i_{\max}} q^i_t \tag{6}$$

where each nonlinear function $k(\cdot)$ and $h(\cdot)$ cite Hatze's parameterized fitting function [26] with two parameters, namely, a_1 and a_2 (see the Appendix).

B. Torque Estimation Model

We consider knee and ankle joint estimation torques $\hat{\tau}_t$ and muscle forces $\mathbf{f}_t$ using the following standard simple linear model:

$$\hat{\tau}_t = \mathbf{w}^\top \mathbf{f}_t \tag{7}$$

where $\mathbf{f}_t = (f^1, \ldots, f^m, 1)^\top$ is the muscle contraction force, and $\mathbf{w} = (w^1, \ldots, w^n, w^0)$ is the model parameter vector of a constant pulley model at knee and ankle joints. These parameters are determined by the least square estimation method to minimize the torque estimation error

$$E = \frac{1}{2}\sum_{t=0}^{N}(\tau_t - \hat{\tau}_t)^2 \tag{8}$$

where the target torque τ_t is derived from the inverse dynamics model, as explained in the following section. N is the number of the training sampling.

C. Floating Base Inverse Dynamics

To derive joint torques from joint angle trajectories, an inverse dynamics model of an approximated subject body is used. However, different from previous studies that worked on estimating knee movements from EMG signals when a subject was sitting on a chair [19], [20], we consider squat movements that are involved in daily behaviors. Therefore, we need to explicitly take the ground reaction forces $\mathbf{f}_{\rm grf}$ into account. For this purpose, we use floating base inverse dynamics

$$\mathbf{M}(\mathbf{q})\ddot{\mathbf{q}} + \mathbf{h}(\mathbf{q}, \dot{\mathbf{q}}) + \mathbf{g}(\mathbf{q}) = \mathbf{S}^\top \boldsymbol{\tau} + \mathbf{J}_c^\top(\mathbf{q})\mathbf{f}_{\rm grf} \tag{9}$$

where $\mathbf{q}$ represents the general coordinate system of the joint angles, $M(\mathbf{q})$ is the floating base inertia matrix, $h(\mathbf{q}, \dot{\mathbf{q}})$ is the floating base centripetal Coriolis, $\mathbf{g}(\mathbf{q})$ is the gravity force, $\mathbf{S}$ is the actuated joint selection matrix, and $\mathbf{J}_c$ is the Jacobian matrix, which represents relationships between joint angle movements and deviations of contact points. If $\mathbf{f}_{\rm grf}$ can be measured by a force sensor, the inverse dynamics torques can be computed from (9). However, this approach is undesirable because the force sensors must be located at all contact points. Therefore, we calculate the torques and the ground reaction forces that correspond to the joint angles, the velocity, and the acceleration by computing the QR decomposition of $\mathbf{J}_c$ [21], i.e.,

$$\mathbf{J}_c^\top = \mathbf{Q}\begin{bmatrix}\mathbf{R}\\ 0\end{bmatrix} \tag{10}$$

where $\mathbf{Q}$ is orthogonal, and $\mathbf{R}$ is an upper triangle matrix of rank k if given rank$(J_c) = k$. We can decompose the dynamics (9) into two independent equations from (10), i.e.,

$$\mathbf{S}_c\mathbf{Q}^\top(\mathbf{M}\ddot{\mathbf{q}} + \mathbf{h} + \mathbf{g}) = \mathbf{S}_c\mathbf{Q}^\top\mathbf{S}^\top\boldsymbol{\tau} + \mathbf{R}\mathbf{f}_{\rm grf} \tag{11}$$

$$\mathbf{S}_u\mathbf{Q}^\top(\mathbf{M}\ddot{\mathbf{q}} + \mathbf{h} + \mathbf{g}) = \mathbf{S}_u\mathbf{Q}^\top\mathbf{S}^\top\boldsymbol{\tau}. \tag{12}$$

Although (11) and (12) are independent, the full dynamics is represented with either equation. Equation (12) describes the full dynamics without ground reaction forces, and the ground reaction forces are computed from (11), where $\mathbf{S} = [\mathbf{I}_{n\times n}\ \mathbf{0}_{n\times 6}]$, $\mathbf{S}_c = [\mathbf{I}_{k\times k}\ \mathbf{0}_{k\times(n+6-k)}]$, and $\mathbf{S}_u = [\mathbf{0}_{(n+6-k)\times k}\ \mathbf{I}_{(n+6-k)\times(n+6-k)}]$. $\mathbf{I}_{n\times n}$ is a unit matrix of the n rows and n columns.

D. Weight Support Force

Finally, the estimated joint torques are converted to the force inputs for the PAM with using joint angle information measured by the goniometers. The measured joint angles are used to derive the Jacobian matrix

$$\mathbf{J} = \begin{bmatrix} \dfrac{\partial y_{\rm hip}}{\partial \theta_{\rm knee}} & \dfrac{\partial y_{\rm hip}}{\partial \theta_{\rm ankle}} \end{bmatrix} \tag{13}$$

where $y_{\rm hip}$ denotes vertical hip position, $\theta_{\rm knee}$ denotes left knee joint angle, and $\theta_{\rm ankle}$ denotes left ankle joint angle (see also Fig. 3). By using the derived Jacobian, we convert the estimated knee and ankle joint torques to the vertical support forces

$$f_{\rm pam} = (\mathbf{J}\mathbf{J}^{\top})^{-1}\mathbf{J} \begin{bmatrix} \hat{\tau}_{\rm knee} \\ \hat{\tau}_{\rm ankle} \end{bmatrix} \tag{14}$$

where $\hat{\tau}_{\rm knee}$ and $\hat{\tau}_{\rm ankle}$ are estimated left knee and ankle torques, respectively.

IV. Experimental Setups

Here, we introduce our experimental setups. In Section IV-A, we explain a calibration procedure of the PAM system. In Section IV-B, we show the four different setups of the squat experiments.

A. Calibrations

1) PAM Pressure to Force Model: At the calibration stage, we obtain load cell variables that measure the actual vertical PAM force, the valve pressure, and the contraction rate by periodically changing the loads. Using the least square method, we estimate the PAM parameters in (2) with using the initial values in (3) and initialize encoder so that we can find an initial length of PAM to calculate PAM contraction rate. For the quadratic regression of (2), we consider forces and contraction rates as inputs and the valve pressure as output. Fig. 2 shows the frequency responses of the PAM-based weight support system. We obtained the data by generating support force with a range from 100 to 300 N. The amplitude error and the phase error are shown in Fig. 2.

2) EMG to Joint Torque Model: The parameter of the tendon-pulley model in (7) was estimated from squat motion data for 30 s with different frequencies and depths. In other words, the number of samples used to find the parameters was $N = 7500$. Fig. 4 shows the placements of EMG electrode and goniometers. We measured EMG signals of the femoral muscle (Channel 1: e^1), the biceps muscle of the thigh (Channel 2: e^2), the vastus medialis muscle (Channel 3: e^3), the vastus lateralis muscle (Channel 4: e^4), the tibialis anterior muscle (Channel 5: e^5), the lateral head of the gastrocnemius muscle (Channel 6: e^6), and the medial head of the gastrocnemius muscle (Channel 7: e^7). The left leg pitch angles of hip, knee, and ankle joints are measured by goniometers. Then, the measured joint angles are used in the floating base inverse dynamics model.

We sample the amplified EMG and goniometer signals with a sampling rate of 250 Hz, i.e., sampling period is $\Delta t = 4$ ms.

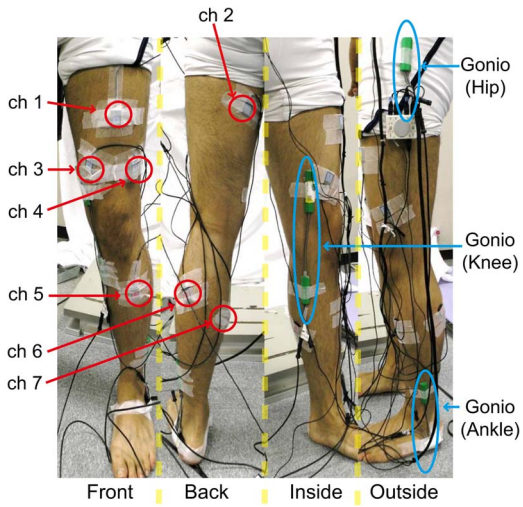

Fig. 4. EMG electrode and goniometer placements.

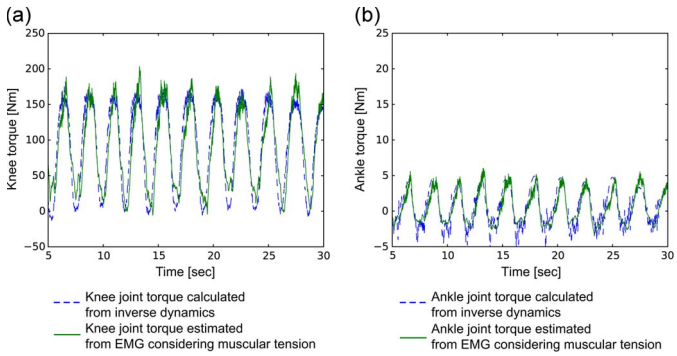

Fig. 5. Torque estimation performances. The estimated (a) knee and (b) ankle joint torques from EMG signals are indicated by solid lines. Target joint torque profiles derived from joint angle trajectory with using floating base inverse dynamics model are plotted by dashed lines. The estimation performances are evaluated with using a test data set that is not used for finding the parameters of the tendon-pulley model in (7).

To estimate the knee joint torque, we compute muscle forces with an augmented input for bias estimation: $\mathbf{f} = (f^1, \ldots, f^7, 1)^{\top}$ from the EMG signals measured by the seven sensor channels. Similarly, the ankle joint torque is estimated by three muscle forces $\mathbf{f} = (f^5, f^6, f^7, 1)^{\top}$. f^1 is derived from the femoral muscle activity, f^2 is from the biceps muscle of the thigh, f^3 is from the vastus medialis muscle, f^4 is from the vastus lateralis muscle, f^5 is from the tibialis anterior muscle, f^6 is from the lateral head of the gastrocnemius muscle, and f^7 is from the medial head of the gastrocnemius muscle. Fig. 5 shows torque estimation performances. This estimation performances are evaluated with using a test data set that is not used for finding the parameters of the tendon-pulley model in (7). The correlation between the predicted knee torques from the EMG signals and target torque trajectories was 0.86, and the root-mean-square error was 33.9 N · m. The correlation coefficient between the predicted ankle torques from the EMG signals and target torque trajectories was 0.86, and the root-mean-square error was 8.62 N · m. These results indicate that our torque estimation method from the EMG signals is useful to control our PAM-based weight support system. Note that, since the knee joint torque is dominant in the squat movement,

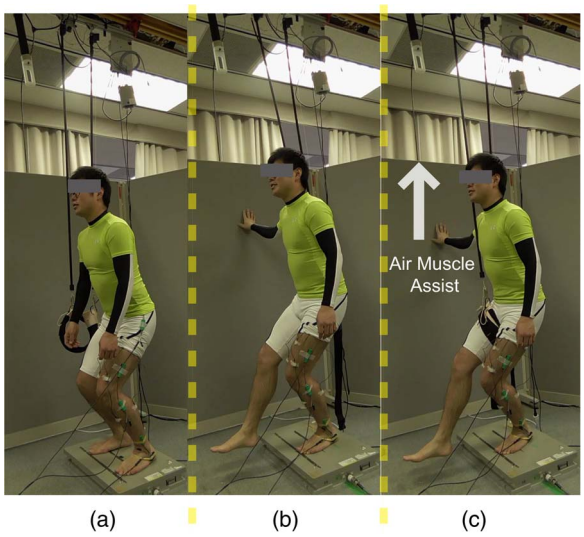

Fig. 6. Experimental setups. (a) Normal two-leg squat. (b) One-leg squat without using the assist system. (c) One-leg squat with the weight support. In experimental setups (b) and (c), subjects are instructed to touch the wall to maintain the balance. (a) Two-leg normal squat. (b) Left leg squat. (c) Left leg squat + assist right side.

we mainly analyze the EMG signals around the knee joint in Section V.

B. Assisting Squat Movements

We compared EMG magnitudes with four different experimental conditions: 1) normal two-leg squat; 2) one-leg squat without the assist system; 3) one-leg squat with EMG-based weight support; and 4) one-leg squat with constant force support, where the constant force is derived as the mean value of target assist force calculated from the floating base inverse dynamics. Fig. 6 shows the three squat experimental setups used for the four different experimental conditions.

We set two different frequencies as lower and upper limits for each squat in order to validate real-time assist performance of the weight support system: 0.2 Hz for the slow dynamic motion and 0.5 Hz for the fast dynamic motion. The lower limit that the subject was able to squat continuously with using one leg without weight assist was decided as 0.2 Hz. The upper limit that was able to be accurately controlled with respect to the response of the valve from the result of PAM calibrations in Section IV-A was 0.5 Hz. Four healthy subjects took part in the experiments (ages 23–30, males). The subjects were instructed to match the timing of squat motion to metronome sound.

V. Results

Here, we show the results of real-time assist performance of the squat movements by using the developed weight support system.

A. Individual Data Analysis

Fig. 7(a) and (b), respectively, shows mean and variance of the knee joint angles of representative subject (subject A) during one cycle of 0.2- and 0.5-Hz squat movements in the four different squat conditions. (c-1)–(c-8) in Fig. 7(c) show the mean and variance of EMG signals measured from the vastus medialis muscle (e^3) and the vastus lateralis muscle (e^4) of subject A during one cycle of 0.2-Hz squat movements in the four different squat conditions, and (c-9) shows the box plot of the corresponding EMG magnitude. (d-1)–(d-8) in Fig. 7(d) show the mean and variance of EMG signals measured from the vastus medialis muscle (e^3) and the vastus lateralis muscle (e^4) of subject A during one cycle of 0.5-Hz squat movements in the four different squat conditions, and (d-9) shows the box plot of the corresponding EMG magnitude. Fig. 7(e) and (f) shows the EMG data of subject B. Fig. 7(g) and (h) shows the EMG data of subject C. Fig. 7(i) and (j) shows the EMG data of subject D. We focused on monitoring these two muscles, i.e., the vastus medialis and vastus lateralis muscles, because these knee-joint related muscles mainly contributed to generate the squat movements. All the EMG profiles in Fig. 7 are low-pass filtered with a cutoff of 2 Hz and full-wave rectified.

As presented in Fig. 7(a) and (b), the subject generated squat movements with similar amplitude and frequency in the four different squat conditions. Fig. 7(c)–(j) shows the amplitudes of EMG signals in the four different squat conditions. These results indicate that the magnitude of EMG signals in the normal and the EMG-based assist conditions is less than that in the one-leg condition, and that in the constant-force-based assist conditions is little less. Table I shows the root mean square (RMS: $\sqrt{(1/T)\int_0^T x(t)^2 dt}$ for 30 s, $T = 30$) of raw EMG signals from seven muscles $(e^1 - e^7)$ with the two different movement frequencies of 0.2 and 0.5 Hz in the four different squat conditions. Results in Table I show that the vastus medialis muscle activities (e^3) and the vastus lateralis muscle activities (e^4) in the normal squat condition (i) and the one-leg squat with EMG-based weight support (iii) are comparable in each subject, whereas these muscle activities are much larger in the one-leg squat without weight support condition (ii). These two muscles in the one-leg squat with constant force support (iv) are also assisted, but not as much as EMG-based weight support.

On the other hand, for the other five muscles, we did not observe consistent differences in EMG signals in the four different experimental conditions among the four subjects (see also Table I). For subject D, we found much larger muscle activities on the tibialis anterior muscle e^5. This is possibly because subject D intensively uses that muscle to maintain the balance during the squat movements.

B. Integrated Data Analysis

Fig. 8(a) and (b) shows the average %MVC of the vastus medialis muscle activities (e^3) and vastus lateralis muscle activities (e^4) with the two different movement frequencies of 0.2 and 0.5 Hz in the four different squat conditions across all subjects. The %MVC is normalized muscle activity (e) for each subject and each muscle separately, by using maximum value of rectified and low-pass filtered EMG signal $(e_{\max})$: $\%\text{MVC} = e/e_{\max}$. This allows comparing among different

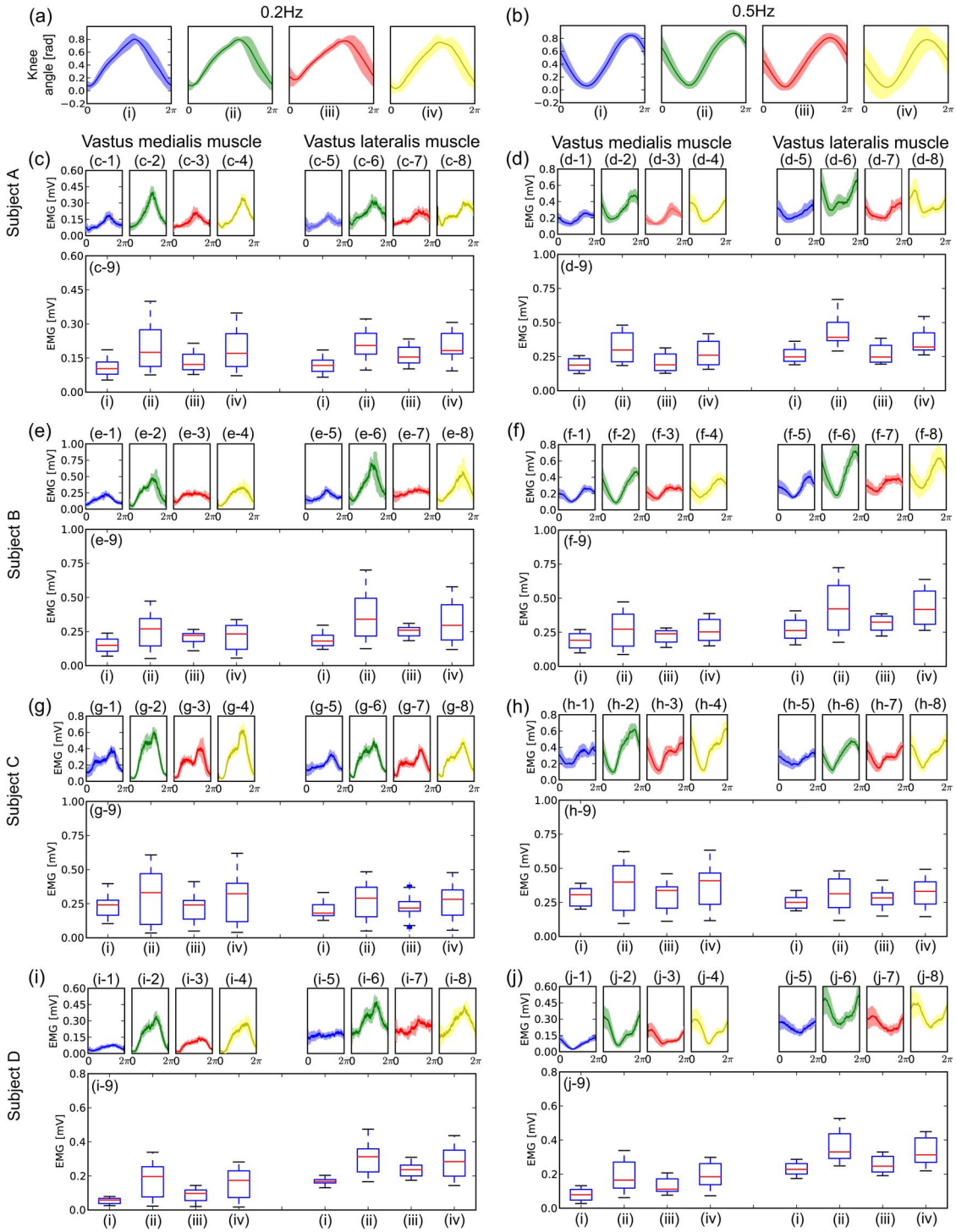

Fig. 7. Squat movement profiles of each subject with frequencies of 0.2 and 0.5 Hz among the four different experimental conditions with box plot. Blue lines show normal squat, green lines show one-leg squat without weight support, red lines show one-leg squat with EMG-based weight support, and yellow lines show one-leg squat with constant force support. (a) and (b) Mean and variance of knee joint angles of representative subject during one cycle of 0.2- and 0.5-Hz squat movements in the four different squat conditions. (c)–(j) Squat movement profiles of the vastus medialis and vastus lateralis muscles with frequencies of 0.2 and 0.5 Hz.

subjects. $e_{\max}$ is the maximum value of the muscle activity e, which is calculated in each experiment and regarded as the muscle activity level of maximum voluntary contraction (MVC) in this study. We applied a t-test to the average %MVC of one-leg squat without the weight support (ii), one-leg squat with the EMG-based weight support (iii), and one-leg squat with the constant force support (iv) with reference to normal two-leg squat (i). We found a significant difference between (i) and (ii) $(p < 0.01)$ and between (i) and (iv) $(p < 0.05)$, but we found no significant difference between (i) and (iii) $(p > 0.05)$ in the 0.2-Hz squat movements. In addition, we also found a significant difference between (i) and (ii) $(p < 0.01)$ and between (i) and (iv) $(p < 0.01)$, but we found no significant difference between (i) and (iii) $(p > 0.05)$ in the 0.5-Hz squat

TABLE I
RMS OF THE RAW EMG SIGNALS

Subject A						**Subject B**					
Squat frequency	**EMG**	**RMS** ($\times 10^{-2}$)				**Squat frequency**	**EMG**	**RMS** ($\times 10^{-2}$)			
		(i)	(ii)	(iii)	(iv)			(i)	(ii)	(iii)	(iv)
0.2 Hz	e^1	5.50	9.61	7.29	8.78	0.2 Hz	e^1	7.29	12.5	8.03	10.0
	e^2	1.78	3.47	2.65	2.30		e^2	3.21	5.00	4.54	4.97
	e^3	**11.9**	22.5	**14.1**	20.5		e^3	**16.0**	29.7	**21.0**	23.5
	e^4	**12.6**	22.1	**16.7**	21.3		e^4	**19.8**	42.2	**25.6**	36.0
	e^5	26.7	8.13	15.9	7.18		e^5	8.57	11.4	9.71	4.47
	e^6	2.29	4.56	3.06	3.08		e^6	5.30	10.1	5.73	4.83
	e^7	2.67	5.95	2.65	2.24		e^7	4.94	12.4	12.9	9.10
0.5 Hz	e^1	11.6	23.2	11.9	16.8	0.5 Hz	e^1	10.6	13.3	9.84	13.7
	e^2	2.80	4.30	3.77	3.70		e^2	3.22	5.03	4.49	4.71
	e^3	**20.0**	33.4	**22.0**	29.3		e^3	**19.8**	30.5	**22.8**	28.7
	e^4	**27.2**	45.5	**28.2**	38.1		e^4	**28.8**	47.7	**32.3**	47.1
	e^5	34.8	16.9	10.1	8.52		e^5	8.08	4.68	8.42	5.08
	e^6	1.65	2.42	2.39	2.70		e^6	7.67	8.90	5.70	8.42
	e^7	1.62	1.73	2.68	2.13		e^7	6.28	12.8	12.7	10.7
Subject C						**Subject D**					
Squat frequency	**EMG**	**RMS** ($\times 10^{-2}$)				**Squat frequency**	**EMG**	**RMS** ($\times 10^{-2}$)			
		(i)	(ii)	(iii)	(iv)			(i)	(ii)	(iii)	(iv)
0.2 Hz	e^1	7.31	12.3	8.91	11.8	0.2 Hz	e^1	7.43	14.6	10.1	14.0
	e^2	3.87	4.22	4.13	4.82		e^2	1.64	4.49	3.33	4.90
	e^3	**25.1**	35.9	**25.5**	35.2		e^3	**5.79**	20.3	**9.68**	18.1
	e^4	**21.5**	30.0	**23.9**	29.2		e^4	**17.1**	31.7	**24.0**	29.6
	e^5	34.6	26.7	19.4	29.6		e^5	85.4	102	102	90.2
	e^6	2.70	5.45	5.74	4.43		e^6	1.87	2.15	2.19	2.08
	e^7	4.00	9.22	9.94	7.50		e^7	7.59	5.55	6.29	7.85
0.5 Hz	e^1	11.3	16.1	12.8	15.6	0.5 Hz	e^1	9.81	16.8	12.5	15.9
	e^2	4.00	5.51	4.37	5.40		e^2	2.22	8.12	4.45	4.88
	e^3	**30.6**	41.5	**32.5**	41.0		e^3	**8.77**	21.1	**14.1**	21.3
	e^4	**26.0**	33.7	**29.2**	34.2		e^4	**23.4**	37.6	**26.5**	34.7
	e^5	30.9	18.4	18.0	18.9		e^5	111	124	102	102
	e^6	2.62	7.38	7.29	6.05		e^6	2.25	2.43	2.15	2.06
	e^7	2.58	7.42	10.6	8.23		e^7	10.1	8.86	5.65	7.38

movements. These results suggest that the developed weight support system can assist the left leg of the subjects with the similar force that the right leg is supposed to generate using a PAM-based weight support system. Our system is controlled by the force estimated from the EMG signals of the left leg, assuming that humans move both left and right legs with the same force while squatting. The constant force support also assisted, but the effectiveness was less than the EMG-based weight support. Consequently, we showed the usefulness of our proposed weight support system for actively assisting subjects by using the measured EMG signals.

VI. CONCLUSION

In this paper, we have introduced our newly developed PAM-based weight support system, which can be controlled by the estimated joint torques with the online EMG measurement. The parameters of the torque estimation model are calibrated with using an inverse dynamics model, which represents physical property of a subject. In particular, we considered using floating base inverse dynamics to explicitly take the ground reaction force into account so that we can treat the movements with both feet on the ground such as squat behaviors. As a concrete example, we applied our developed system to assist squat movement. The results show that muscle activities measured from vastus medialis and vastus lateralis muscles EMG signals were not significantly different between one-leg squat with the EMG-based weight support and normal two-leg squat, whereas the differences between normal two-leg squat and one-leg squat and between normal two-leg squat and one-leg squat with the constant force support were significant. As an application, this system can possibly be used for partial weight bearing therapies. Concretely, it can possibly be used for compensating the disabled side of the body for the early stage of therapies. Then, the vertical component force can be gradually decreased as the patient recovers lower body motor functions.

Since the PAM-based weight support system is lightweight and safe, has high power-weight ratio, and is easy to attach

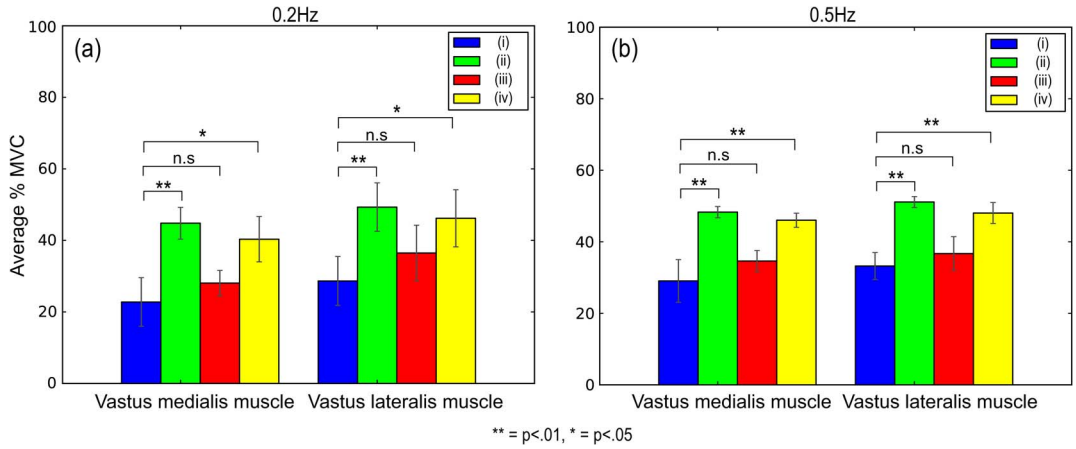

Fig. 8. Statistical comparisons with bar plots of the vastus medialis muscle and the vastus lateralis muscle %MVC across all subjects. Blue bars show the normal squat movement, green bars show the one-leg squat movement without weight support, red bars show the one-leg squat movement with EMG-based weight support, and yellow bars show the one-leg squat movement with constant force support. (a) 0.2-Hz squat movement. (b)0.5-Hz squat movement.

to the ceiling or a small gantry, the system can potentially be useful not only for rehabilitation but also for industrial applications.

Although we focused on assisting one particular movement, i.e., squatting, it would be possible to apply our weight support system to assist other kinds of movements such as stepping or walking by using the estimated torque from EMG signals with considering phase difference between the left leg and right leg movements. Moreover, we can possibly use our developed weight support system with constant assist force to simply compensate the gravity, but with much wider movement range than existing devices so that the weight support system can help a therapist when the therapist is nearby a patient. This gravity compensation strategy can be also useful for the industrial applications, such as the load carriage assistance.

To further improve the force control performance of the weight support, it can be beneficial to explicitly take hysteresis model of the PAM into account. In addition, in this study, we used load cells only for the calibration and did not use it for force feedback control since there is delay in the air-pressure-based control system. However, using the load cell feedback for online adaptation of the parameters of the weight support system would be one of the interesting directions as a part of future study.

APPENDIX

In this appendix, we explain the Hill–Stroeve model used in (6). $h(\eta^i, \xi^i)$ and $k(\xi^i)$ are computed as follows:

$$h(\eta^i, \xi^i) = \frac{1 + \tanh(a_1 \dot{\eta}^i - a_2)}{b_2} - b_1 e^{-2.6(\xi^i - 1)} \quad (15)$$

$$k(\xi^i) = 0.32 + 0.71 e^{-1.112(\xi^i - 1)} \times \sin\left(3.722(\xi^i - 0.656)\right) \quad (16)$$

where $\xi^i = (l^i(\theta)/l^{i,n})$ and $\eta^i = (\dot{\xi^i(\theta)}/v^{i,\max})$, $v^{i,\max} = 3.0$, $l^i(\theta)$ is the current length of muscle i, $l^{i,n}$ is its natural length, and $v^{i,\max}$ is its maximum contraction rate. In this paper, the natural muscle length is approximately set as the same to the link length. The current muscle length is computed by adding partial periphery length of the joint pulley to the natural muscle length with considering the current joint angle. $b_1 = [1 - \tanh\{a_1(1 + a_2)\}]/b_2$, and $b_2 = \tanh\{a_1(1 + a_2)\}$. The parameters a_1 and a_2 depend on the muscle type, and the approximate range of values for a_1 and a_2 are $a_1 = 1.6{-}2.7$ and 2.9–3.8 and $a_2 = -0.05{-}0.1$ and -0.01–0.1 for fast and slow fibers, respectively. In this paper, we defined these parameters for each muscles experimentally by repeating the cross-validation to minimize the error of torque estimation. The $\overline{f_{\max}}$ for the muscles were determined anatomical information [27]; and we used $\overline{f^1_{\max}} = 975$ N, $\overline{f^2_{\max}} = 3000$ N, $\overline{f^3_{\max}} = 2250$ N, $\overline{f^4_{\max}} = 2250$ N, $\overline{f^5_{\max}} = 1125$ N, $\overline{f^6_{\max}} = 1875$ N, and $\overline{f^7_{\max}} = 1875$ N.

REFERENCES

[1] K. Suzuki, G. Mito, H. Kawamoto, Y. Hasegawa, and Y. Sankai, "Intention-based walking support for paraplegia patients with robot suit HAL," *Adv. Robot.*, vol. 21, no. 12, pp. 1441–1469, Dec. 2007.

[2] S. K. Au, P. Dilworth, and H. Herr, "An ankle-foot emulation system for the study of human walking biomechanics," in *Proc. IEEE Int. Conf. Robot. Autom.*, 2006, pp. 2939–2945.

[3] T. Kagawa and Y. Uno, "Gait pattern generation for a power-assist device of paraplegic gait," in *Proc. 18th Int. Symp. Robot Human Interactive Commun.*, 2009, pp. 633–638.

[4] C. Fleischer and G. Hommel, "A human–exoskeleton interface utilizing electromyography," *IEEE Trans. Robot.*, vol. 24, no. 4, pp. 872–882, Aug. 2008.

[5] S.-H. Hyon, J. Morimoto, T. Matsubara, T. Noda, and M. Kawato, "XoR: Hybrid drive exoskeleton robot that can balance," in *Proc. IEEE/RSJ Int. Conf.*, Sep. 25–30, 2011, pp. 2715–2722.

[6] T. Noda *et al.*, "Brain-controlled exoskeleton robot for BMI rehabilitation," in *Proc. IEEE-RAS Int. Conf. Humanoid Robots*, 2012, pp. 21–27.

[7] A. Hildebrandt, O. Sawodny, R. Neumann, and A. Hartmann, "Cascaded control concept of a robot with two degrees of freedom driven by four artificial pneumatic muscle actuators," in *Proc. Amer. Control Conf.*, 2005, pp. 680–685.

[8] S. Maeda, N. Tsujiuchi, T. Koizumi, M. Sugiura, and H. Kojima, "Development and control of pneumatic robot arm for industrial fields," in *Proc. 37th IEEE IECON/IECON*, Nov. 2011, pp. 86–91.

[9] J. Ueda, D. Ming, V. Krishnamoorthy, M. Shinohara, and T. Ogasawara, "Individual muscle control using an exoskeleton robot for muscle function testing," *IEEE Trans. Neural Syst. Rehabil. Eng.*, vol. 18, no. 4, pp. 339–350, Aug. 2010.

[10] H. Kobayashi, "Development on wearable robot for human power support," in *Proc. 28th IEEE IECON/IECON*, Nov. 2002, vol. 4, pp. 3091–3096.

[11] K. Gordon and D. Ferris, "Learning to walk with a robotic ankle exoskeleton," *J. Biomech.*, vol. 40, no. 12, pp. 2636–2644, 2007.
[12] C. Kinnaird and D. Ferris, "Medial gastrocnemius myoelectric control of a robotic ankle exoskeleton," *IEEE Trans. Neural Syst. Rehabil. Eng.*, vol. 17, no. 1, pp. 31–37, Feb. 2009.
[13] S. Lee and Y. Sankai, "Power assist control for walking aid with HAL-3 based on EMG and impedance adjustment around knee joint," in *Proc. IEEE/RSJ Int. Conf. Intell. Robots Syst.*, 2002, vol. 2, pp. 1499–1504.
[14] T. Hayashi, H. Kawamoto, and Y. Sankai, "Control method of robot suit HAL working as operator's muscle using biological and dynamical information," in *Proc. IEEE/RSJ Int. Conf. IROS*, 2005, pp. 3063–3068.
[15] J. Son, S. Hwang, and Y. Kim, "An EMG-based muscle force monitoring system," *J. Mech. Sci. Technol.*, vol. 24, no. 10, pp. 2099–2105, Oct. 2010.
[16] H. He and K. Kiguchi, "A study on EMG-based control of exoskeleton robots for human lower-limb motion assist," in *Proc. 6th Int. Spec. Topic Conf. ITAB*, 2007, pp. 292–295.
[17] K. Kiguchi and Y. Imada, "EMG-based control for lower-limb power-assist exoskeletons," in *Proc. IEEE Workshop RIISS*, 2009, pp. 19–24.
[18] G. S. Sawicki and D. P. Ferris, "A pneumatically powered Knee-Ankle-Foot Orthosis (KAFO) with myoelectric activation and inhibition," *J. Neuroeng. Rehab.*, vol. 6, no. 1, p. 23, Jun. 2009.
[19] C. Fleischer and G. Hommel, "Calibration of an EMG-based body model with six muscles to control a leg exoskeleton," in *Proc. IEEE Int. Conf. Robot. Autom.*, 2007, pp. 2514–2519.
[20] D. G. Lloyd and T. F. Besier, "An EMG-driven musculoskeletal model to estimate muscles forces and knee joint moments in vivo," *J. Biomech.*, vol. 36, no. 6, pp. 765–776, Jun. 2002.
[21] M. Mistry, J. Buchli, and S. Schaal, "Inverse dynamics control of floating base systems using orthogonal decomposition," in *Proc. IEEE ICRA*, 2010, pp. 3406–3412.
[22] A. Hill, "The heat of shortening and the dynamic constants of muscle," *Proc. R. Soc. Lond. A, Biol. Sci.*, vol. 126, no. 843, pp. 136–195, Oct. 1938.
[23] S. Stroeve, "Learning combined feedback and feedforward control of a musculoskeletal system," *Biol. Cybern.*, vol. 75, no. 1, pp. 73–83, Jul. 1996.
[24] K. Inoue, "Rubbertuators and applications for robots," in *Proc. 4th Int. Symp. Robot. Res*., Cambridge, MA, USA: MIT Press, 1988, pp. 57–63.
[25] D. Caldwell, A. Razak, and M. Goodwin, "Braided pneumatic muscle actuators," in *Proc. IFAC Conf. Intell. Auton. Veh.*, 1993, pp. 507–512.
[26] H. Hatze, "A myocybernetic control model of skeletal muscle," *Biol. Cybern.*, vol. 25, no. 2, pp. 103–119, Jan. 1977.
[27] S. Hanawa, K. Santo, K. Hiramoto, T. Iwami, and Y. Shimada, "Muscle tension estimation of the lower extremities using EMG data," (in Japanese), in *Proc. 244th Tohoku Local Conf. Soc. Instrum. Control Eng.*, 2008, pp. 244–243.

Jun-ichiro Furukawa received the B.E. and M.S. degrees from Osaka University, Osaka, Japan, in 2011 and 2013, respectively. He is currently working toward the Ph.D. degree in the Graduate School of Frontier Biosciences, Osaka University.

He is also currently with the Department of Brain Robot Interface, ATR Computational Neuroscience Laboratories, Kyoto, Japan. His research interests include machine learning, biosignal processing, computational neuroscience, brain–machine interface, and robotics.

Tomoyuki Noda received Ph.D. degree in engineering from Osaka University, Osaka, Japan, 2009.

In 2009, he joined the Institute for Neural Computation, University of California, San Diego, La Jolla, CA, USA, as a Visiting Research Scholar. He has been a Postdoctoral Researcher with ATR Computational Neuroscience Laboratories, Kyoto, Japan, since 2010.

Dr. Noda was the recipient of the Best Video Nominate at IEEE AAAI 2008, the Best Video at LAB-RS 2008, in a development of a whole-body humanoid robot with tactile sensation and compliant joints, and the Best Paper Nominate Award at IEEE Humanoids 2012 in BMI controlled exoskeleton.

Tatsuya Teramae received the Ph.D. degree in engineering from Tottori University, Tottori, Japan, in 2011.

He is currently a Researcher with the Department of Brain Robot Interface, ATR Computational Neuroscience Laboratories, Kyoto, Japan. His research interests are optimal control and human–machine interface.

Dr. Teramae is a member of The Society of Instrument and Control Engineers of Japan and The Institute Of Electrical Engineers of Japan.

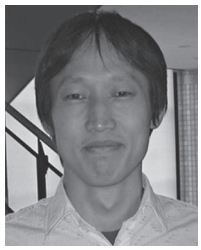

Jun Morimoto received the Ph.D. degree in information science from Nara Institute of Science and Technology, Nara, Japan, in 2001.

From 2001 to 2002, he was a Postdoctoral Fellow with The Robotics Institute, Carnegie Mellon University, Pittsburgh, PA, USA. Since 2002, he has been with Advanced Telecommunications Research Institute International (ATR), Kyoto, Japan, where he was a Researcher in the Computational Brain Project, the International Cooperative Research Project, Japan Science and Technology Agency from 2004 to 2009 and is currently the Head of the Department of Brain Robot Interface, ATR Computational Neuroscience Laboratories.